Desalination and Water Treatment
www.deswater.com

doi: 10.1080/19443994.2013.806224

52 (2014) 1937–1946
February

Taylor & Francis
Taylor & Francis Group

Covalent bonding synthesis of magnetic graphene oxide nanocomposites for Cr(III) removal

Huai Li[a], Zifang Chi[b,c], Jianzheng Li[a,*]

[a]*State Key Laboratory of Urban Water Resource and Environment, Harbin Institute of Technology, Harbin 150090, P.R. China*
Tel./Fax: +86 0451 86283761; email: ljz6677@163.com
[b]*College of Environment and Resources, Jilin University, Changchun 130021, P.R. China*
[c]*State Environmental Protection Key Laboratory of Microorganism Application and Risk Control (MARC), Tsinghua University, Beijing 100084, P.R. China*

Received 19 February 2013; Accepted 12 May 2013

ABSTRACT

A covalent bonding technique to obtain magnetic graphene oxide nanocomposites (Fe_3O_4/SiO_2–GO) decorated with core/shell nanoparticles is reported. Fe_3O_4/SiO_2–GO was characterized by transmission electron microscopy, energy dispersive X-ray spectrometer, X-ray diffraction, Fourier transform infrared, Raman, and thermogravimetric analysis techniques. Through covalent synthesis method, magnetic core/shell particles in size of 20–40 nm were homogeneously dispersed onto graphene oxide. The characteristic Si–O–Si peak (1091, 468 cm^{-1}), Fe–O (576 cm^{-1}), and aromatic C=C (1621 cm^{-1}) were the direct evidences to consolidate the formation of the Fe_3O_4/SiO_2–GO. The DTG curve showed about 54.45 wt% of metal oxide deposited on the surface of GO. The adsorption behaviors, including adsorption kinetics and isotherms parameters, effect factors, and mechanisms of chromium adsorption on Fe_3O_4/SiO_2–GO were studied. Fe_3O_4/SiO_2–GO demonstrated an extremely fast Cr(III) removal from the wastewater within 5 min and could be separated faster by using a permanent magnet. The adsorption kinetics followed the pseudo-second-order model and Fe_3O_4/SiO_2–GO exhibited better Cr(III) removal efficiency in solutions with high pH (>3). The adsorption of Cr(III) fits the Freundlich equation well. Based on abundant oxygen functional groups and negative surface charge on Fe_3O_4/SiO_2–GO, the adsorption mechanisms could be explained as electrostatic interactions and ion exchange. The significantly reduced treatment time required to remove the Cr(III) and the applicability in treating the solutions with high pH made Fe_3O_4/SiO_2–GO promise for the efficient removal of heavy metals from the leather industry wastewater.

Keywords: Graphene oxide; Fe_3O_4/SiO_2–GO; Covalent synthesis; Adsorption; Cr(III) removal

1. Introduction

The leather industry has led to an increased discharged wastewater containing heavy metals (Cr (III)) that have detrimental effects on the environment and human health. The maximum permissible limit of

---

*Corresponding author.

When the above article was first published online, the order of authors' names was incorrect. This version has been amended. Please see Erratum [10.1080/19443994.2013.817372]

the total Cr in leather industry effluent has been recommended as 1.5 mg/L by the Ministry of Environmental Protection, China [1]. With better awareness of these problems, a number of technologies to remove Cr have been developed, including electrochemical precipitation [2], reverse osmosis [3], ion exchange (IE) [4], and adsorption [5,6]. However, most of these methods require further treatment and the operation cost is high. Consequently, adsorption is an alternative favorable and feasible approach because of its low cost and high efficiency [5,7,8].

Carbon-based nanomaterials have been studied as superior adsorbents for their potential environmental applications to remove pollutants, such as organic pollutants and metals with high capacity and selectivity in aqueous solutions [9–11]. One of the advantages of carbon-based nanoparticles (NPs) as attractive adsorbents is that they have much larger specific surface areas [12]. Graphene oxide (GO), a product of graphite from an oxidization process, is an ideal material for wastewater treatment. GO is also water-soluble with low conductivity [13]. The oxidation of graphite to GO can introduce abundant oxygen functional groups on GO surface that can be used as anchoring sites for metal ion complexation, making it a potential material as a super adsorbent [14]. Magnetite NPs (Fe_3O_4) have been widely utilized in biological and environmental applications because they have unique magnetic properties and allow the rapid separation of target molecules from the samples simply by applying an appropriate magnetic field [15–17]. Integration of magnetic NPs and GO into a hybrid material has recently become a hot topic of research because of its new and/or enhanced functionalities, and therefore, it holds a great promise for wider applications in catalysis, biomedical fields, adsorption, and separation, etc. [18].

However, there are some disadvantages in the process of production and application: (1) formation of Fe_3O_4–GO is usually achieved by in situ reduction of iron salt precursors or assembly of the magnetic NPs on GO surface. Fe_3O_4 NPs are attached to a GO layer only by physical adsorption or electrostatic interaction, so they may be easily leached out from the GO sheets during application [19], (2) high temperature is needed in situ reduction of iron salt precursors. For example, Shen et al. [20] synthesized GO–magnetic nanoparticle composites by attaching magnetic NPs to GO through a high temperature reaction of ferric triacetylacetonate with GO in 1-methyl-2-pyrrolidone. Recently, Cong et al. [21] prepared magnetic-functionalized reduced GO sheets via high-temperature decomposition of $Fe(acac)_3$ precursor in polyol, (3) it is a challenge to precisely control the loading amount of Fe_3O_4 and then tailor the properties of resultant hybrids for desired application [19], and (4) another major challenge is because of its easy oxidation/dissolution of the pure Fe NPs when using these nanomaterials, especially in acidic solutions.

To protect the magnetic NPs against oxidation, a shell structure is often introduced, including silica [22], polymer [23], and noble metals [24,25]. And recently, covalent functionalizing agents have been used to modify graphene by an amidation reaction which can provide better stability, accessibility, selectivity, and less leaching [26,27]. He et al. [19] reported a two-step process to fabricate hybrids of GO nanosheets and surface-modified Fe_3O_4 NPs which could not only be used as an effective adsorbent for removing cationic dyes in water but could also be used to prepare magnetic GO films.

In this study, magnetic GO nanocomposites were developed by covalently immobilizing magnetic core/shell Fe_3O_4/SiO_2 on GO surfaces to settle the problems above. The materials were characterized by transmission electron microscopy (TEM), energy dispersive spectroscopy (EDS), powder X-ray diffraction (XRD), Fourier transform infrared spectroscopy (FTIR), Raman spectrometer, and thermogravimetric analysis (TGA). The effects of the treatment time, adsorbent loading, and pH values on the Cr(III) removal were investigated for the prepared Fe_3O_4/SiO_2–GO. The adsorption kinetics and isotherms were also investigated by fitting the experimental data with different models and the removal mechanism was proposed.′

2. Materials and methods

2.1. Preparation of Fe_3O_4/SiO_2-NH_2 NPs

Fe_3O_4 magnetic NPs were prepared using the chemical co-precipitation method [28]. Fe_3O_4/SiO_2 microspheres were prepared according to the method reported with some modifications [29,30]. Typically, the previously synthesized Fe_3O_4 ferrofluid (4 mL) was diluted with 100 mL water–ethanol (1:4, v/v) solution followed by the addition of 2.5 mL ammonia solution (25 wt%) and 1.0 mL TEOS [CAS: 78-10-4] sequentially. The mixture was reacted for 12 h at room temperature under continuous stirring.

Then, (3-aminopropyl) triethoxysilane (APS) [CAS: 919-30-2] was added to the reaction mixture and the mixture was stirred for another 24 h at 40°C. The silica-coated magnetic NPs grafted with APS were collected by magnetic separation using a magnet and washed several times with deionized water and ethanol. The material obtained was referred to as $Fe_3O_4/SiO_2–NH_2$ NPs.

2.2. Synthesis of Fe_3O_4/SiO_2-GO

GO, prepared from natural graphite by the modified Hummer's method [31], was used as the starting material for the fabrication of Fe_3O_4/SiO_2–GO. First, a mixture of 0.2 g GO in 60 mL water was ultrasonicated for 3 h for GO exfoliation and then 10 mg of 1-ethyl-3-(3-dimethylaminopropyl)carbodiimide (EDC) [CAS: 25952-53-8] and 8 mg of N-hydroxysuccinnimide (NHS) [CAS: 6066-82-6] were added into the solution of the exfoliated GO. The above mixture was stirred for 30 min and ultrasonicated for another 30 min to form a homogenous suspension. Next, 0.2 g of Fe_3O_4/SiO_2 NPs was added into the suspension and the mixture was subjected to ultrasonication for 30 min. Finally, the reaction was carried out at 80℃ for 1 h under stirring. Fe_3O_4/SiO_2–GO was obtained by magnetic separation and washed with water for several times.

2.3. Characterization

The samples were characterized by TEM (JEOL 2011, 200 kV), EDS, Raman spectrometer (Jobin Yvon HR 800, with laser excitation at 457.9 nm), and FTIR (Avatar 360, with a resolution of 2 cm^{-1}). The TGA was performed by heating the samples in a nitrogen or air flow at a rate of 100 mL/min using a Perkin–Elmer Diamond TG/DTA thermal analyzer with a heating rate of 10℃/min. XRD patterns of all samples were obtained on a Bruker D8-Advance X-ray diffractometer with Cu Kα radiation ($k = 1.5418$ Å) at accelerating voltage and current of 40 kV and 40 mA, respectively. The concentration of chromium ions was analyzed using Perkin-Elmer 3110 atomic absorption spectrometry, a Thermo Scientific ICAP 6000 Series ICP system.

2.4. Adsorption measurement

The chromic nitrate solution containing 10 mg/L chromium was treated with Fe_3O_4/SiO_2–GO. Briefly, the chromium solution was mixed with predetermined amount of Fe_3O_4/SiO_2–GO to the concentrations of Fe_3O_4/SiO_2–GO (0.25, 1.0, 2.0, 2.5, and 3.0 g/L) [32]. The mixture was shaken continuously at room temperature for 50 min. Then, Fe_3O_4/SiO_2–GO was separated from the solutions by using a permanent magnet. The clear solutions were then collected and subjected to ICP analysis to determine the final chromium concentrations. For the kinetic study, the Fe_3O_4/SiO_2–GO concentration was maintained at 1 g/L in the original pH (5.8) solution for different adsorption time such as 5, 10, 15, 25, 35, and 50 min. (Because $Cr(OH)_2^+$ was the dominant species at medium acidity between pH 4.0 and 6.5 instead of $Cr(OH)_3$ at higher pH (>6.5) according to Sperling et al.[33], the initial pH 5.8 was chosen when Cr(III) was removed by adsorption only rather than precipitation). The pH study was conducted at different pH values from 1 to 9; the pH value was adjusted by adding hydrochloric acid or sodium hydroxide solutions. To perform an adsorption isotherm analysis, the Fe_3O_4/SiO_2–GO concentration was maintained at 1 g/L in the original pH solution for different concentrations of chromium solution (in a plastic vial), such as 2.5, 5, 10, 20, and 40 mg/L, at room temperature (25 ± 2℃) for 50 min.

3. Results and discussion

3.1. Microstructure investigation

3.1.1. TEM and EDS analysis

TEM measurements providing further insights into the morphology and structure of the NPs are shown in Fig. 1(a). These particles were of sphere-like morphology in general, and the diameter was ranging from 20 to 40 nm. The TEM image also showed that NPs were aggregated because of the magnetic dipolar interaction among the magnetite NPs. The sample was nearly in core/shell structures, black spots showing Fe_3O_4, and ash part as SiO_2 shell. This indicated the successful synthesis of magnetic core/shell particles. The spherical Fe_3O_4 NPs had an average diameter of 10 nm, and the SiO_2 shells were approximately 20 nm in thickness. As illustrated in Fig. 1(c), the presence of $Fe_3O_4/SiO_2–NH_2$ NPs was confirmed by EDS analysis, which indicated that besides Au peaks from the sputtered layer prior to SEM analysis, only Fe, Si, and O were detected. Based on the above results, it proved that the SiO_2 particles existed on the outer shell of raspberry-like magnetic hollow silica nanospheres. The inorganic compound-functionalized iron oxide NPs could greatly enhance the antioxidation properties of naked Fe_3O_4 NPs and its corresponding scope of application would be greatly extended as they are very promising for catalysis, separation et al. [26].

With the aid of NHS and EDC, Fe_3O_4/SiO_2–GO NPs were obtained from the condensation reaction between the amino group of Fe_3O_4/SiO_2 and carboxylic group of GO, which formed a carboxamide bonding [19]. Fig. 1(b) shows typical TEM images of Fe_3O_4/SiO_2–GO. It could be observed that the graphene sheets were distributed between the loosely

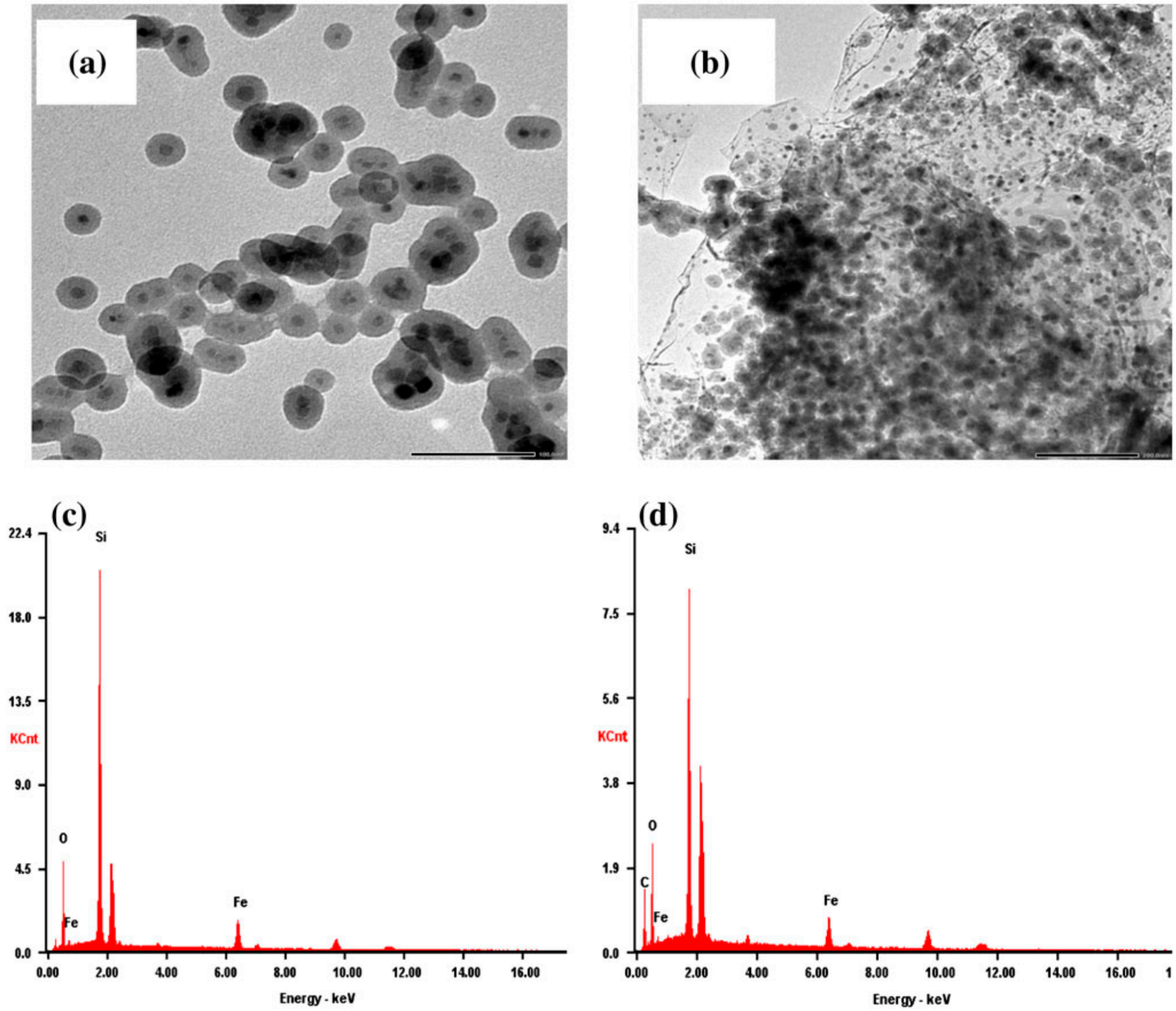

Fig. 1. TEM images (a, b) and EDS (c, d) for Fe_3O_4/SiO_2–NH_2 and Fe_3O_4/SiO_2–GO.

packed Fe_3O_4 NPs and that a large amount of void spaces formed on the material, which could prevent the aggregation of Fe_3O_4 NPs to a certain extent. Moreover, even after a long time of sonication, the Fe_3O_4 NPs were still strongly anchored on the surface of the graphene sheets with a high density (not shown) implying the strong interaction between Fe_3O_4 NPs and graphene sheets [34]. The signal of C was present on Fe_3O_4/SiO_2–GO, which demonstrated the graft of Fe_3O_4/SiO_2 onto the surface of GO Fig. 1(d).

3.1.2. XRD analysis

The XRD patterns of GO, magnetite, Fe_3O_4/SiO_2–NH_2, and Fe_3O_4/SiO_2–GO are shown in Fig. 2. GO showed a sharp peak centered at $2\theta = 10.6^\circ$, corresponding to the (0 0 2) interplanar spacing of 0.84 nm. XRD peak of GO (1 0 0) crystal at $2\theta = 42^\circ$ also appeared. The characteristic peak of pristine graphite at $2\theta = 26.4^\circ$ did not disappear completely after strong oxidation, which may be due to the restacking of GO by the role of the van der Waals forces. In general, these data suggested that graphite was successfully converted to GO after oxidation by Hummer's method. For Fe_3O_4 NPs, diffraction peaks with 2θ at 30.4°, 35.6°, 43.3°, 53.4°, 57.3°, 62.8°, and 74.1° were observed, which were ascribed to the (2 2 0), (3 1 1), (4 0 0), (4 2 2), (5 1 1), (4 4 0), and (5 3 3) planes of the magnetite, Fe_3O_4, which were in accord with pure spinel Fe_3O_4 (ICDD file no. 65-3107), indicative of a cubic spinel structure of the magnetite. Diffraction peaks of SiO_2 (2 0 1) at 23.4° was also observed indicating the structure of SiO_2 (ICDD file

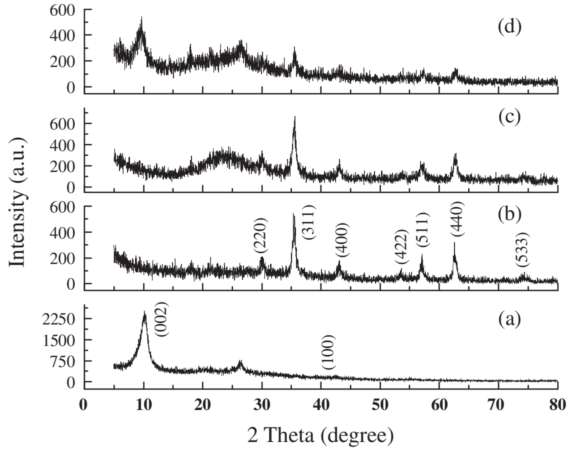

Fig. 2. XRD patterns of (a) GO, (b) Fe_3O_4, (c) Fe_3O_4/SiO_2–NH_2, and (d) Fe_3O_4/SiO_2–GO.

no. 50-0511) coated on the Fe_3O_4 NPs. Compared with Fe_3O_4/SiO_2–NH_2 NPs, the same sets of characteristic peaks were also observed for Fe_3O_4/SiO_2–GO indicating the stability of the crystalline phase of Fe_3O_4 NPs in the composites. Compared with (0 0 2) diffraction peak of GO, the diffraction peak intensity of Fe_3O_4/SiO_2–GO at $2\theta = 10.3^\circ$ was obviously reduced and the XRD peak of GO (1 0 0) crystal at $2\theta = 42^\circ$ totally disappeared. These results suggested that the layered GO had been exfoliated largely and more disordered stacking and less agglomerated graphene sheets were presented in the composite [35]. The as-prepared Fe_3O_4/SiO_2–GO hybrid composite presented diffraction peaks of the Fe_3O_4/SiO_2 combined with GO. Additionally, there were no apparent shifts in the diffraction peaks. These results indicated that the Fe_3O_4/SiO_2 NPs were well-loaded on the GO sheets and the loading of Fe_3O_4/SiO_2 NPs did not affect the GO sheets packing from the layered structure during all the experimental processes.

3.1.3. FTIR analysis

FTIR spectra of GO, Fe_3O_4, Fe_3O_4/SiO_2–NH_2, and Fe_3O_4/SiO_2–GO NPs are shown in Fig. 3. In the spectrum of GO, C–H (2,976 cm^{-1}), C=O (1,725 cm^{-1}), aromatic C=C (1,621 cm^{-1}), and alkoxy C–O (1,045 cm^{-1}) stretching vibrations were observed. As illustrated, the absorption band at 578 cm^{-1} corresponded to the Fe–O stretching bond for Fe_3O_4 NPs. The characteristic adsorption peaks of Fe_3O_4/SiO_2–NH_2 at 1,631, 1,087, 952, and 466 cm^{-1}, which were attributed to NH deformation vibration modes, the Si–O–Si and Si–O–H stretching vibration, respectively, verified the formation of the silica shell. The characteristic Si–O–Si peak (1,091, 468 cm^{-1}), Fe–O (576 cm^{-1}), and aromatic C=C (1,621 cm^{-1}) were the direct evidences to consolidate the formation of the Fe_3O_4/SiO_2–GO. It was generally accepted that the interpretation of surface groups could only be qualitative, as they could not be expected to behave as isolated functional groups [34].

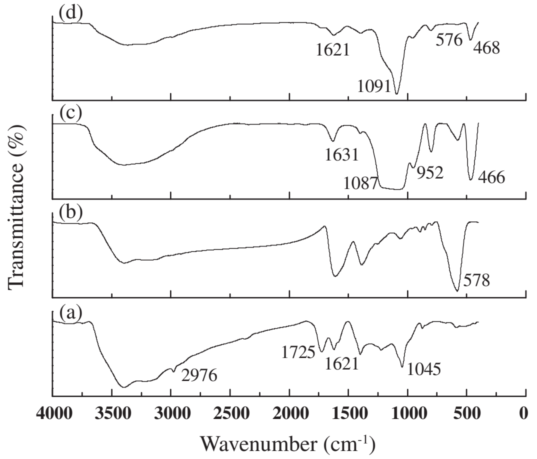

Fig. 3. FT-IR spectra of (a) GO, (b) Fe_3O_4, (c) Fe_3O_4/SiO_2–NH_2, and (d) Fe_3O_4/SiO_2–GO.

3.1.4. Magnetic separation analysis

The Fe_3O_4/SiO_2–GO was dispersed in water with a concentration of 20 mg/mL by sonication for several minutes. The sample could be uniformly dispersed in deionized water forming a stable brown-black suspension. When a magnet was set close to the glass vial containing the magnetic NPs dispersed in deionized water, the NPs were attracted toward the magnet very quickly and accumulated to the side of the glass vial near the magnet within seconds, resulting in a clear and transparent solution. Removing the external magnetic field and sonicating the solution, the magnetic NPs could be rapidly dispersed again in solution. Thus, the attraction and dispersion processes could be readily altered by applying and removing an external magnetic field, showing good water dispersion and magnetic separation [36]. This property was essentially important for the convenient recycling of Fe_3O_4/SiO_2–GO.

3.1.5. TG–DTA analysis

Thermal properties of Fe_3O_4/SiO_2–GO NPs were investigated with TG–DTA analysis, which was performed in nitrogen and air atmosphere at a heating rate of 10 °C min^{-1}. As shown in Fig. 4(a), there were two weight loss stages in nitrogen atmosphere. An abrupt weight loss occurred from 120 to 280˚C, which could be assigned for the removal of labile oxygen-containing functional groups as CO, CO_2, and H_2O vapors from the sample caused by the destruction of the oxygenated functional groups [37]. Correspondingly, the DTG curve showed a strong exothermal peak centered at 207.8˚C. From 280 to 800˚C, Fe_3O_4/SiO_2–GO showed much higher thermal stability with a gradual weight loss and no abrupt weight loss. The weight loss was usually attributed to the loss of the residual (or adsorbed) solvent and the decomposition of residual organic functional groups on graphene sheets [38]. In contrast with the results of the sample in nitrogen atmosphere, the TG/DTA curves of Fe_3O_4/SiO_2–GO in air atmosphere (Fig. 4(b)) presented characteristic step/peaks in the range from 280 to 500˚C. Correspondingly, the DTG curve showed one strong exothermal peak centered at 466˚C. It could be assigned for the decomposition of carbon skeleton and decomposition of aminopropyl groups grafted to the silica surface [30]. According to the mass loss on Fe_3O_4/SiO_2–GO, about 54.45 wt% of metal oxide deposited on the surface of GO, which was close to the starting ratio of Fe_3O_4 and GO.

3.1.6. Raman analysis

Fig. 5 shows Raman spectra of GO and Fe_3O_4/SiO_2–GO. In two samples, two prominent peaks were clearly visible, corresponding to the so-called G peak, which corresponded to the Brillouin-zone-centered LO-phonon around 1,575 cm^{-1}, and D peak, which corresponded to the double-resonance excitation of phonons close to the K point in the Brillouin zone around 1,360 cm^{-1} [39]. The intensity ratio (I_D/I_G) was characteristic of the extent of disorder present within in the material [40,41]. For our samples, the I_D/I_G ratios of the GO and Fe_3O_4/SiO_2–GO were, respectively, 0.246 and 0.673 reflecting the increase in disorder. Moreover, there was only a little increase in intensity ratio which confirmed the presence of donor molecules on graphene [42]. By comparing the G-bands of GO and Fe_3O_4/SiO_2–GO, it was clear that G-band of Fe_3O_4/SiO_2–GO occurred at 1,576 cm^{-1}, which was upshifted by 9 cm^{-1} compared with that of GO. The Raman shifts of the G band for Fe_3O_4/SiO_2–GO provided evidence for the charge transfer between the GO sheets and Fe_3O_4/SiO_2, which suggested a strong interaction between the Fe_3O_4/SiO_2 and the GO sheet.

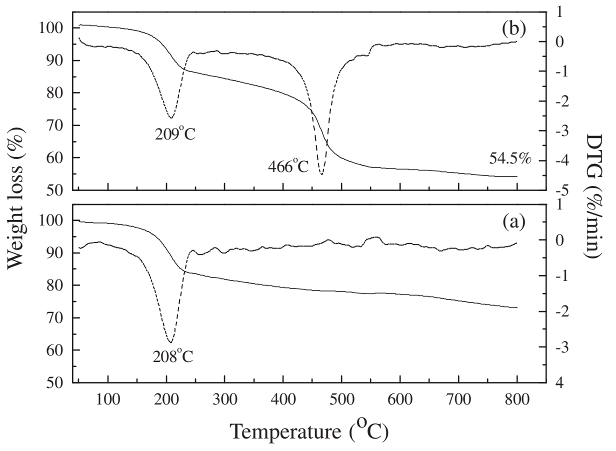

Fig. 4. TG and DTG curves of Fe_3O_4/SiO_2–GO: (a) in nitrogen atmosphere and (b) in air atmosphere.

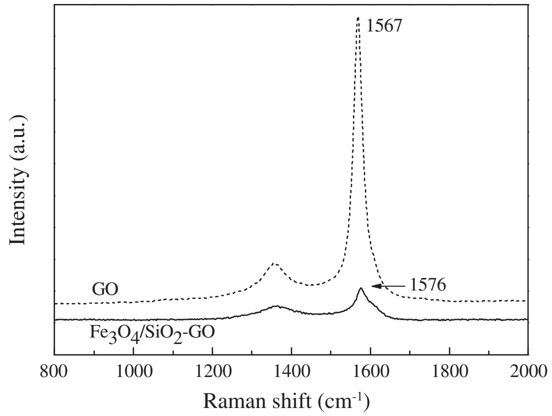

Fig. 5. Raman spectra of GO and Fe_3O_4/SiO_2–GO NPs.

3.2. Chromium removal

To achieve good extraction and recoveries towards the target ions, the Cr(III) removal percentages treated by different concentrations of Fe_3O_4/SiO_2–GO (0–3 g/L) under shaking continuously for 50 min were shown in Fig. 6. The removal percentages of chromium increased rapidly when the concentrations of Fe_3O_4/SiO_2–GO increased from 0.25 to 3 g/L, indicating that the Fe_3O_4/SiO_2–GO NPs had large enrichment ability towards chromium. Considering the detection sensitivity and consumption of Fe_3O_4/SiO_2–GO, the testing concentration of 1 g/L was employed in the studies (Fig. 6).

The adsorption of Cr(III) on the Fe_3O_4/SiO_2–GO was a surface reaction. It could be predicted that the pH played an important role in the adsorption of particular metal ions onto Fe_3O_4/SiO_2–GO [10,43]. The Cr (III) removal efficiencies by Fe_3O_4/SiO_2–GO in different pH solutions were shown in Fig. 7 with an initial Cr(III) concentration of 10 mg/L. The adsorption was weak at low pH values ($pH < 3$), but the adsorption increased with the pH values increasing from 3 to 9.

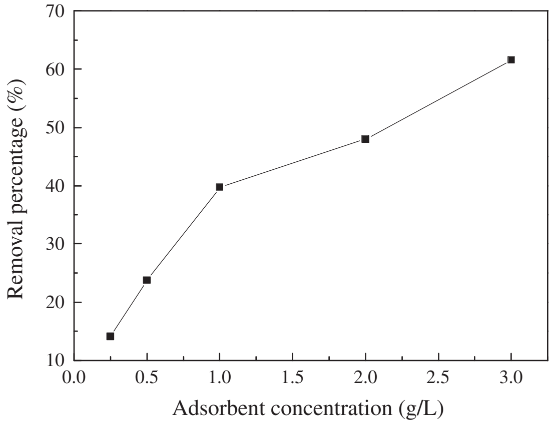

Fig. 6. Cr(VI) removal percentage based on different loadings of Fe_3O_4/SiO_2–GO. ([Cr(III)] = 10 mg/L, pH 5.8, treatment time: 50 min).

In an acidic solution, the species of surface groups were –COOH and –OH, respectively. The decrease in pH led to neutralization of surface charge, and thus, the adsorption of cations would decrease. In addition, there were some competitions on −COO− and −O− sites between proton and metal cations in an acidic condition, which would result in a lower adsorption capacity. The increase in the pH values of the solution would convert more of above groups to −COO− and −O−, and provide electrostatic interactions that were favorable for adsorbing Cr(III) and other cationic species.

3.3. Adsorption kinetics and isotherms

Fig. 8 shows the Cr(III) adsorption data over Fe_3O_4/SiO_2–GO at intervals. It was observed that the equilibrium adsorption capacities could be obtained nearly within 5 min. Quantifying the changes in adsorption with time required an appropriate kinetic model, pseudo-first-order [44], pseudo-second-order [45], Elovich [46], and intraparticle diffusion [47] kinetic models were investigated and compared.

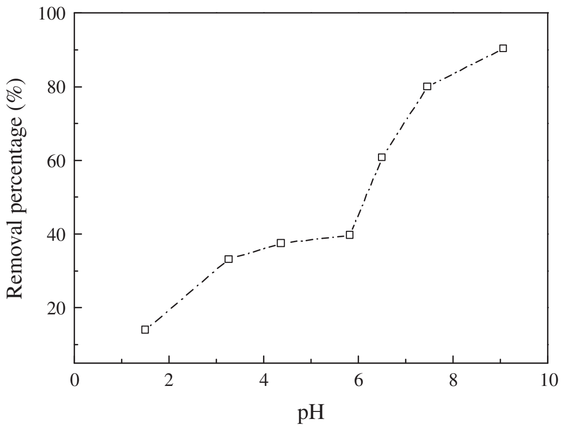

Fig. 7. Effect of solution pH values on Cr(III) removal efficiency of Fe_3O_4/SiO_2–GO. ([Fe_3O_4/SiO_2–GO] = 1 g/L, [Cr(III)] = 10 mg/L, treatment time: 50 min).

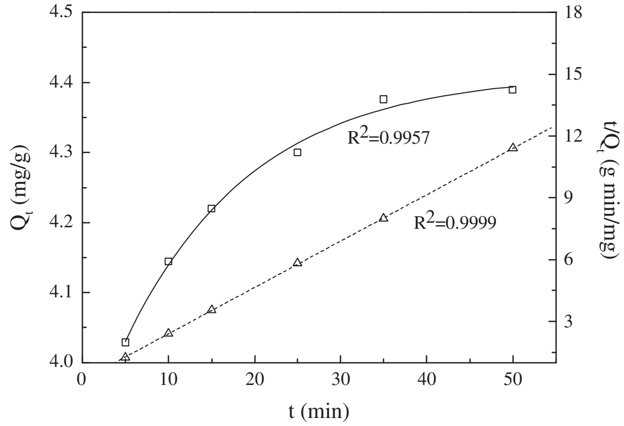

Fig. 8. Kinetic adsorption data plots of Cr(III) by Fe_3O_4/SiO_2–GO: Cr(III) removal rate Q_t vs. time t (square line) and the transformed rate plot t/Q_t vs. t (triangle line). (([Fe_3O_4/SiO_2–GO] = 1 g/L, [Cr(III)] = 10 mg/L, pH 5.8).

The fitting results obtained from different models were summarized in Table 1. With the highest correlation coefficient of $R^2 = 0.9999$ (fitting curve is shown in Fig. 8, square symbol curve), pseudo-second-order model provided an excellent correlation for the adsorption of Cr(III) on Fe_3O_4/SiO_2–GO. The higher adsorption rate constant k_{ad} (0.32 g/mg/min) of Fe_3O_4/SiO_2–GO from the pseudo-second-order model than that of the aluminum magnesium mixed with hydroxide (<0.024 g/mg/min) [48], pomegranate husk carbon (<0.032 g/mg/min) [49], magnetic graphene nanocomposites (0.28 g/mg/min) [32], and active carbon (<0.093 g/mg/min) [50] confirmed further the much faster removal rate of the Fe_3O_4/SiO_2–GO.

The isotherm models of Linear, Langmuir, and Freundlich [5] were applied to fit the adsorption equilibrium data of Cr(III) on Fe_3O_4/SiO_2–GO. The fitting results obtained from different models were summarized in Table 1. With the highest correlation coefficient of $R^2 = 0.9758$, Freundlich model provided an excellent correlation for the adsorption of Cr(III) on Fe_3O_4/SiO_2–GO. When the Cr(III) concentration increased, the adsorption amount first increased sharply, then increased slightly, and finally reached saturation. The maximum adsorption capacities of Cr (III) on Fe_3O_4/SiO_2–GO was 4.7 mg/g at the Fe_3O_4/SiO_2–GO concentration of 1 g/L. The Freundlich constant n was found to be greater than 1, which was a favorable condition for adsorption. Thus, it was implicated that the strong affinity of Fe_3O_4/SiO_2–GO towards chromium developed in this work could

Table 1
Parameters obtained from different kinetic and isotherm models ([Fe_3O_4/SiO_2–GO] = 1 g/L; pH 5.8)[a]

Models	Equation	Parameters		R^2
Pseudo-first-order	$\log(Q_e - Q_t) = \log Q_e - \frac{k_1}{2.303}t$	k_1 (min^{-1}) 0.10	Q_e (mg/g) 0.73	0.9374
Pseudo-second-order	$\frac{t}{Q_t} = \frac{1}{k_{ad}Q_e^2} + \frac{t}{Q_e}$	k_{ad} (g/mg/min) 0.32	Q_e (mg/g) 4.45	0.9999
Elovich	$Q_t = \frac{1}{\beta}\ln(\alpha\beta) + \frac{1}{\beta}\ln(t)$	α (mg/g/min) 8008.76	β (g/mg) 2.64	0.989
Intraparticle diffusion	$Q_t = k_{dif}t^{0.5} + C$	k_{dif} (mg/g/$min^{0.5}$) 0.076	C (mg/g) 3.90	0.9421
Linear	$q_e = K_D C_e$	K_D (L/g) 0.0867		0.8476
Langmuir	$\frac{1}{q_e} = \frac{1}{q_{max}} + \frac{1}{q_{max}K_l C_e}$	q_{max} (mg/g) 4.7	K_l (L/mg) 2.48	0.9309
Freundlich	$\log q_e = \log K_F + \frac{1}{n}\log C_e$	K_F (mg/g $(mg/L)^n$) 2.83	n 5.09	0.9758

[a] Q_t is the solid-phase loading of Cr(III) in the adsorbent at time t, Q_e is the adsorption capacity at equilibrium, k_1 is the rate constant of pseudo-first-order adsorption. In pseudo-second-order model, k_{ad} is the rate constant of adsorption. α and β represent the initial adsorption rate and desorption constant in Elovich model. k_{dif} indicates the intraparticle diffusion rate constant and C provide information about the thickness of the boundary layer. In linear model, q_e is the adsorption capacity at equilibrium, C_e is the equilibrium concentration of metals. K_D is often referred to as the partition coefficient of linear model. In Langmuir model, q_{max} is the adsorption capacity of metals on adsorbent, K_l is the Langmuir adsorption constant, which is related to the adsorption energy. K_F and n are Freundlich constants related to adsorption capacity and adsorption intensity, respectively.

serve as an efficient adsorbent for the decontamination of chromium in leather industry effluent treatment.

3.4. Removal mechanism

The adsorption mechanism of Cr(III) on Fe_3O_4/SiO_2–GO was a combined process of Cr(III) together with the SiO_2 outer shell and bare area of GO [32]. Generally speaking, the adsorption of metal ions was based on the three adsorption mechanisms: electrostatic interactions, IE, and complex formation [51]. As we all know, the basic sites as C π electrons on graphene sheets were considered as the important adsorption sites [52]. But GO sheets, not or very less containing delocalized π electrons, and chromium ion/hydrogen ion could not form the electron donor–acceptor complexes. The surface charge was regarded as negative because of abundant oxygen functional groups on GO surface. According to Madadrang et al., [53] GO surface is negatively charged in all test pH ranges (2–12) due to the functional groups of GO that can be ionized to make GO negative in solutions. Two IE processes were also responsible for the removal of Cr(III) with Fe_3O_4/SiO_2–GO: IE reaction between Cr (III) and −COOH or −OH groups as shown below:

(1) Cr(III) reacts with –COOH and –OH groups on GO surface to form a complex

$GO\text{–}COOH + Cr^{3+} \rightarrow GO\text{–}COO^-\text{–}Cr^{3+} + H^+$
$(GO\text{–}COOH)_2 + Cr^{3+} \rightarrow (GO\text{–}COO^-)_2\text{–}Cr^{3+} + 2H^+$
$(GO\text{–}COOH)_3 + Cr^{3+} \rightarrow (GO\text{–}COO^-)_3\text{–}Cr^{3+} + 3H^+$
$GO\text{–}OH + Cr^{3+} \rightarrow GO\text{–}O^-\text{–}Cr^{3+} + H^+$
$(GO\text{–}OH)_2 + Cr^{3+} \rightarrow (GO\text{–}O^-)_2\text{–}Cr^{3+} + 2H^+$
$(GO\text{–}OH)_3 + Cr^{3+} \rightarrow (GO\text{–}O^-)_3\text{–}Cr^{3+} + 3H^+$

(2) Cr(III) may also react with –OH groups of Fe_3O_4/SiO_2 to form a complex

$Fe_3O_4/SiO_2\text{–}OH + Cr^{3+} \rightarrow Fe_3O_4/SiO_2\text{–}O^-\text{–}Cr^{3+} + H^+$
$(Fe_3O_4/SiO_2\text{–}OH)_2 + Cr^{3+} \rightarrow (Fe_3O_4/SiO_2\text{–}O^-)_2\text{–}Cr^{3+} + 2H^+$
$(Fe_3O_4/SiO_2\text{–}OH)_3 + Cr^{3+} \rightarrow (Fe_3O_4/SiO_2\text{–}O^-)_3\text{–}Cr^{3+} + 3H^+$

The above reaction mechanism is supported by the pH change when the Fe_3O_4/SiO_2–GO is mixed with a Cr(III) solution. The reaction between −COOH and −OH with Cr(III) releases proton into the solution and then decreases the pH value of the solution, similar to the results Madadrang et al. reported [53].

Consequently, electrostatic interaction between Cr (III) ions and negative surface charge and/or IE could be regarded as the main interaction for the adsorption of Cr(III) ion onto Fe_3O_4/SiO_2–GO.

4. Conclusions

In summary, the magnetic GO nanocomposites decorated with core/shell NPs was synthesized via a covalent bonding method. The results demonstrated the successful graft of Fe_3O_4/SiO_2 onto the surface of GO. The adsorption of Cr(III) fits the Freundlich equation well and the constant n was found to be greater than 1, which was a favorable condition for adsorption. The pseudo-second-order kinetic model best described the adsorption behavior of Cr(III) on Fe_3O_4/SiO_2–GO. The materials showed their highest adsorption capacity at relatively higher pH value solutions. The adsorption mechanisms on Fe_3O_4/SiO_2–GO could be explained as electrostatic interactions and IE. Fe_3O_4/SiO_2–GO exhibited a bright future for their applications in toxic heavy metal removal from the leather industry wastewater.

Acknowledgments

This work was financially supported by State Key Laboratory of Urban Water Resource and Environment, Harbin Institute of Technology (Grant No. 2010DX06), National Natural Science Foundation of China (No. 51178136), and State Environmental Protection Key Laboratory of Microorganism Application and Risk Control (No. MARC2012D009).

References

[1] Z.R. Guo, G.M. Zhang, J.D. Fang, X.D. Dou, Enhanced chromium recovery from tanning wastewater, J. Clean Prod. 14 (2006) 75–79.

[2] N. Kongsricharoern, C. Polprasert, Chromium removal by a bipolar electro-chemical precipitation process, Water Sci. Technol. 34 (1996) 109–116.

[3] A. Hafez, S. El-Manharawy, Design and performance of the two-stage/two-pass RO membrane system for chromium removal from tannery wastewater. Part 3, Desalination 165 (2004) 141–151.

[4] F.J. Alguacil, I. Garcia-Diaz, F. Lopez, The removal of chromium (III) from aqueous solution by ion exchange on Amberlite 200 resin: Batch and continuous ion exchange modelling, Desalin. Water Treat. 45 (2012) 55–60.

[5] D. Zhang, S.Y. Wei, C. Kaila, X. Su, J. Wu, A.B. Karki, D.P. Young, Z.H. Guo, Carbon-stabilized iron nanoparticles for environmental remediation, Nanoscale 2 (2010) 917–919.

[6] Y. Zhao, J.R. Peralta-Videa, M.L. Lopez-Moreno, M.H. Ren, G. Saupe, J.L. Gardea-Torresdey, Kinetin increases chromium absorption, modulates its distribution, and changes the activity of catalase and ascorbate peroxidase in Mexican Palo Verde, Environ. Sci. Technol. 45 (2011) 1082–1087.

[7] J.K. Yang, H.J. Park, H.D. Lee, S.M. Lee, Removal of Cu(II) by activated carbon impregnated with iron(III), Colloids Surf., A 337 (2009) 154–158.

[8] M. Imamoglu, O. Tekir, Removal of copper(II) and lead(II) ions from aqueous solutions by adsorption on activated carbon from a new precursor hazelnut husks, Desalination 228 (2008) 108–113.

[9] J.P. Ruparelia, S.P. Duttagupta, A.K. Chatterjee, S. Mukherji, Potential of carbon nanomaterials for removal of heavy metals from water, Desalination 232 (2008) 145–156.

[10] B. Tawabini, S. Al-Khaldi, M. Atieh, M. Khaled, Removal of mercury from water by multi-walled carbon nanotubes, Water Sci. Technol. 61 (2010) 591–598.

[11] K. Pyrzynska, M. Bystrzejewski, Comparative study of heavy metal ions sorption onto activated carbon, carbon nanotubes, and carbon-encapsulated magnetic nanoparticles, Colloids Surf. A 362 (2010) 102–109.

[12] M.A. Atieh, O.Y. Bakather, B. Al-Tawbini, A.A. Bukhari, F.A. Abuilaiwi and M.B. Fettouhi, Effect of carboxylic functional group functionalized on carbon nanotubes surface on the removal of lead from water, Bioinorg. Chem. Appl. 2010 (2010) 1–9.

[13] S. Park, J.H. An, I.W. Jung, R.D. Piner, S.J. An, X.S. Li, A. Velamakanni, R.S. Ruoff, Colloidal suspensions of highly reduced graphene oxide in a wide variety of organic solvents, Nano Lett. 9 (2009) 1593–1597.

[14] D.R. Dreyer, S. Park, C.W. Bielawski, R.S. Ruoff, The chemistry of graphene oxide, Chem. Soc. Rev. 39 (2010) 228–240.

[15] M. Faraji, Y. Yamini, M. Rezaee, Magnetic nanoparticles: Synthesis, stabilization, functionalization, characterization, and applications, J. Iran. Chem. Soc. 7 (2010) 1–37.

[16] S. Laurent, D. Forge, M. Port, A. Roch, C. Robic, L.V. Elst, R.N. Muller, Magnetic iron oxide nanoparticles: Synthesis, stabilization, vectorization, physicochemical characterizations, and biological applications, Chem. Rev. 108 (2008) 2064–2110.

[17] Y. Maeda, T. Yoshino, T. Matsunaga, Novel nanocomposites consisting of *in vivo*-biotinylated bacterial magnetic particles and quantum dots for magnetic separation and fluorescent labeling of cancer cells, J. Mater. Chem. 19 (2009) 6361–6366.

[18] Y. Zhang, B.A. Chen, L.M. Zhang, J. Huang, F.H. Chen, Z.P. Yang, J.L. Yao, Z.J. Zhang, Controlled assembly of Fe_3O_4 magnetic nanoparticles on graphene oxide, Nanoscale 3 (2011) 1446–1450.

[19] F.A. He, J.T. Fan, D. Ma, L.M. Zhang, C. Leung, H.L. Chan, The attachment of Fe_3O_4 nanoparticles to graphene oxide by covalent bonding, Carbon 48 (2010) 3139–3144.

[20] J.F. Shen, Y.Z. Hu, M. Shi, N. Li, H.W. Ma, M.X. Ye, One step synthesis of graphene oxide-magnetic nanoparticle composite, J. Phys. Chem. C 114 (2010) 1498–1503.

[21] H.P. Cong, J.J. He, Y. Lu, S.H. Yu, Water-soluble magnetic-functionalized reduced graphene oxide sheets: In situ synthesis and magnetic resonance imaging applications, Small 6 (2010) 169–173.

[22] J.H. Zhu, S.Y. Wei, N. Haldolaarachchige, D.P. Young, Z.H. Guo, Electromagnetic field shielding polyurethane nanocomposites reinforced with core-shell Fe-silica nanoparticles, J. Phys. Chem. C 115 (2011) 15304–15310.

[23] S. Shin and J. Jang, Thiol containing polymer encapsulated magnetic nanoparticles as reusable and efficiently separable adsorbent for heavy metal ions, Chem. Commun. 41 (2007) 4230–4232.

[24] S.J. Cho, J.C. Idrobo, J. Olamit, K. Liu, N.D. Browning, S.M. Kauzlarich, Growth mechanisms and oxidation resistance of gold-coated iron nanoparticles, Chem. Mater. 17 (2005) 3181–3186.

[25] Z.H. Lu, M.D. Prouty, Z.H. Guo, V.O. Golub, C. Kumar, Y.M. Lvov, Magnetic switch of permeability for polyelectrolyte microcapsules embedded with Co@Au nanoparticles, Langmuir 21 (2005) 2042–2050.

[26] T.T. Baby, S. Ramaprabhu, SiO_2 coated Fe_3O_4 magnetic nanoparticle dispersed multiwalled carbon nanotubes based amperometric glucose biosensor, Talanta 80 (2010) 2016–2022.

[27] T. Sainsbury, D. Fitzmaurice, Templated assembly of semiconductor and insulator nanoparticles at the surface of covalently modified multiwalled carbon nanotubes, Chem. Mater. 16 (2004) 3780–3790.

[28] Y.H. Deng, C.C. Wang, J.H. Hu, W.L. Yang, S.K. Fu, Investigation of formation of silica-coated magnetite nanoparticles via sol-gel approach, Colloids Surf. A 262 (2005) 87–93.

[29] C.L. Wu, H. He, H.J. Gao, G. Liu, R.J. Ma, Y.L. An, L.Q. Shi, Synthesis of Fe_3O_4@SiO_2@polymer nanoparticles for controlled drug release, Sci. China Chem. 53 (2010) 514–518.

[30] J.H. Wang, S.R. Zheng, Y. Shao, J.L. Liu, Z.Y. Xu, D.Q. Zhu, Amino-functionalized Fe_3O_4@SiO_2 core-shell magnetic nanomaterial as a novel adsorbent for aqueous heavy metals removal, J. Colloid Interface Sci. 349 (2010) 293–299.

[31] T. Hartono, S.B. Wang, Q. Ma, Z.H. Zhu, Layer structured graphite oxide as a novel adsorbent for humic acid removal from aqueous solution, J. Colloid Interface Sci. 333 (2009) 114–119.

[32] J.H. Zhu, S.Y. Wei, H.B. Gu, S.B. Rapole, Q. Wang, Z.P. Luo, N. Haldolaarachchige, D.P. Young, Z.H. Guo, One-pot synthesis of magnetic graphene nanocomposites decorated with core@double-shell nanoparticles for fast chromium removal, Environ. Sci. Technol. 46 (2012) 977–985.

[33] M. Sperling, S.K. Xu, B. Welz, Determination of chromium (III) and chromium(VI) in water using flow injection on-line preconcentration with selective adsorption on activated alumina and flame atomic absorption spectrometric detection, Anal. Chem. 64 (1992) 3101–3108.

[34] G. Wang, T. Liu, X.L. Xie, Z.Y. Ren, J.B. Bai, H. Wang, Structure and electrochemical performance of Fe_3O_4/graphene nanocomposite as anode material for lithium-ion batteries, Mater. Chem. Phys. 128 (2011) 336–340.

[35] Z.S. Wu, W.C. Ren, L. Wen, L.B. Gao, J.P. Zhao, Z.P. Chen, G.M. Zhou, F. Li, H.M. Cheng, Graphene anchored with Co_3O_4 nanoparticles as anode of lithium ion batteries with enhanced reversible capacity and cyclic performance, Acs Nano 4 (2010) 3187–3194.

[36] C. Hui, C.M. Shen, J.F. Tian, L.H. Bao, H. Ding, C. Li, Y.A. Tian, X.Z. Shi, H.J. Gao, Core-shell Fe_3O_4@SiO_2 nanoparticles synthesized with well-dispersed hydrophilic Fe_3O_4 seeds, Nanoscale 3 (2011) 701–705.

[37] C. Xu, X. Wang, J. Zhu, X.J. Yang, L.D. Lu, Deposition of Co_3O_4 nanoparticles onto exfoliated graphite oxide sheets, J. Mater. Chem. 18 (2008) 5625–5629.

[38] Z.Y. Ji, X.P. Shen, Y. Song, G.X. Zhu, In situ synthesis of graphene/cobalt nanocomposites and their magnetic properties, Mater. Sci. Eng. B 176 (2011) 711–715.

[39] C. Thomsen, S. Reich, Doable resonant Raman scattering in graphite, Phys. Rev. Lett. 85 (2000) 5214–5217.

[40] W.S. Choi, S.H. Choi, B. Hong, D.G. Lim, K.J. Yang, J.H. Lee, Effect of hydrogen plasma pretreatment on growth of carbon nanotubes by MPECVD, Mater. Sci. Eng. C 26 (2006) 1211–1214.

[41] K.N. Kudin, B. Ozbas, H.C. Schniepp, R.K. Prud'homme, I.A. Aksay, R. Car, Raman spectra of graphite oxide and functionalized graphene sheets, Nano Lett. 8 (2008) 36–41.

[42] A.K. Manna, S.K. Pati, Tuning the electronic structure of graphene by molecular charge transfer: A computational study, Chem. Asian J. 4 (2009) 855–860.

[43] S.S. Zhao, D.X. Ma, Preparation of $CoFe_2O_4$ nanocrystallites by solvothermal process and its catalytic activity on the thermal decomposition of ammonium perchlorate, J. Nanomater. 2010 (2010) 1–5.

[44] S. Lagergren, About the theory of so-called adsorption of soluble substances, Kungliga Svenska Vetenskapsakademiens Handlingar 24 (1898) 1–39.

[45] Y.S. Ho, G. McKay, D.A.J. Wase, C.F. Forster, Study of the sorption of divalent metal ions on to peat, Adsorpt. Sci. Technol. 18 (2000) 639–650.

[46] R.S. Juang, M.L. Chen, Application of the Elovich equation to the kinetics of metal sorption with solvent-impregnated resins, Ind. Eng. Chem. Res. 36 (1997) 813–820.

[47] S.K. Srivastava, R. Tyagi, N. Pant, Adsorption of heavy metal ions on carbonaceous material developed from the waste slurry generated in local fertilizer plants, Water Res. 23 (1989) 1161–1165.

[48] Y.J. Li, B.Y. Gao, T. Wu, D.J. Sun, X. Li, B. Wang, F.J. Lu, Hexavalent chromium removal from aqueous solution by adsorption on aluminum magnesium mixed hydroxide, Water Res. 43 (2009) 3067–3075.

[49] A. El Nemr, Potential of pomegranate husk carbon for Cr(VI) removal from wastewater: Kinetic and isotherm studies, J. Hazard. Mater. 161 (2009) 132–141.

[50] A. Ei-Sikaily, A. El Nemr, A. Khaled, O. Abdelwehab, Removal of toxic chromium from wastewater using green alga *Ulva lactuca* and its activated carbon, J. Hazard. Mater. 148 (2007) 216–228.

[51] C. Moreno-Castilla, M.A. Alvarez-Merino, L.M. Pastrana-Martinez, M.V. Lopez-Ramon, Adsorption mechanisms of metal cations from water on an oxidized carbon surface, J. Colloid Interface Sci. 345 (2010) 461–466.

[52] M. Machida, T. Mochimaru, H. Tatsumoto, Lead(II) adsorption onto the graphene layer of carbonaceous materials in aqueous solution, Carbon 44 (2006) 2681–2688.

[53] C.J. Madadrang, H.Y. Kim, G.H. G, N. Wang, J. Zhu, H. Feng, M. Gorring, M.L. Kasner, S.F. Hou, Adsorption behavior of EDTA-graphene oxide for Pb (II) removal, Appl. Mater. Interfaces 4 (2012) 1186–1193.